

Growth and characterization of PbI₂-decorated ZnO nanowires for photodetection applications

Edgars Butanovs^{*}, Sergei Piskunov, Aleksejs Zolotarjovs, Boris Polyakov

Institute of Solid State Physics, University of Latvia, Kengaraga Street 8, Riga, LV-1063, Latvia

abstract

In this study, we demonstrated for the first time the growth of ZnO nanowires (NWs) decorated with highly crystalline few-layer PbI₂ and fabricated two-terminal single-nanowire photodetector devices to investigate the photoelectric properties of the hybrid nanostructures. We developed a novel two-step growth process for uniform crystalline PbI₂ nanosheets via reactive magnetron deposition of a lead oxide film followed by subsequent iodination to PbI₂ on a ZnO NW substrate, and we compared as-grown hybrid nanostructures with ones prepared via thermal evaporation method. ZnO@PbI₂ NWs were characterized by scanning and transmission electron microscopy, X-ray diffraction analysis and photo-luminescence measurements. By fabricating two-terminal single-nanowire photodetectors of the as-grown ZnO@PbI₂ nanostructures, we showed that they exhibit reduced dark current and decreased photoresponse time in comparison to pure ZnO NWs and have responsivity up to 0.6 A/W. Ab initio calculations of the electronic structure of both PbI₂ nanosheets and ZnO NWs have been performed, and show potential for photoelectrocatalytic hydrogen production. The obtained results show the benefits of combining layered van der Waals materials with semiconducting NWs to create novel nanostructures with enhanced properties for applications in optoelectronics or X-ray detectors.

1. Introduction

The surface plays an exceptionally important role in determining nanomaterial physical and chemical properties. The impact of surface modification on nanoscale material properties has been intensively explored for the last few decades [1e3]. Nanowires (NWs) are one-dimensional (1D) nanomaterials that exhibit promising properties beneficial for integration in functional devices, such as photodetectors, nanolasers, LEDs, etc. [4,5], and modification of their surface can significantly improve their electrical, optical and mechanical characteristics [3,4,6]. Modification or decoration of a NW surface has no restrictions of material lattice mismatch and its caused stress at the interface, unlike the conventional thin film growth [5,7,8], therefore, opening new possibilities to engineer novel hybrid nanostructures with desired properties, such as photon detection capability in a broad spectral range [9]. Currently, most research in this field is focused on developing precisely controllable nanostructure fabrication

methods and tuning nanostructure properties for specific applications [6,7,9].

Zinc oxide (ZnO) is one of the most commonly studied NW materials due to its simple synthesis and wide field of applications, such as ultraviolet photodetectors [10,11] and piezoelectric nano-generators [12], as well as the potential to be a scintillator material for X-ray detectors [13e15]. ZnO is an n-type semiconductor with a direct bandgap around 3.2e3.4 eV and it has a high exciton binding energy (60 meV), which allows room temperature excitonic emission [16]. ZnO NWs have frequently been used as template material for nanomaterial synthesis [17,18]. Furthermore, in several studies, it has been demonstrated that passivating the surface of ZnO nanostructures or decorating the NWs with specifically selected materials enhances light and gas detecting properties [19e24].

Lead (II) iodide (PbI₂) is a photoconductor material with 2.2e2.55 eV bandgap [25] and is typically employed in fabricating perovskite solar cells and photodetectors [26e30], and as an X-ray and g-ray detector material [31e34]. PbI₂ has a layered structure in which the covalently bonded IePbI repeating layers are bound by weak van der Waals (vdW) interaction [35]. Recently, it has gained more attention due to the extensive research on various 2D vdW materials, such as graphene and transition metal dichalcogenides

[36,37]. There are theoretical and experimental studies that show band structure shift from direct bandgap to indirect bandgap when the PbI₂ thickness is reduced from bulk to monolayer [35,38], as opposed to well-studied vdW materials, MoS₂, for example [39]. Therefore, monolayer PbI₂ is not expected to be an efficient material for optoelectronics applications. In the last few years, there have been several studies that demonstrate the growth of few-layer PbI₂ crystals and investigate their promising photodetection properties both on rigid and flexible substrates [25,35,40e42]. The growth of 1D PbI₂ NWs for high-sensitivity photodetector applications has also been reported [43]. Zhang et al. proposed low-temperature heteroepitaxial growth of PbI₂ thin film on submeter-sized graphene/polyethylene terephthalate (PET) substrate and showed its applicability in light detection [44]. However, there are challenges remaining in obtaining highly-crystalline and uniform large-area PbI₂ films.

Alternatively, NWs can be used as a template for growth and easier manipulation of layered vdW materials, such as WS₂ and MoS₂, while maintaining the high crystallinity of the materials used and even enhancing their properties [20,45e47]. Large-scale printing of NWs at specified locations on flexible substrates via roll-to-roll transfer has been demonstrated [48], therefore enabling the advancement of all-printed layered material- and NW-based electronic and optoelectronic devices in the future. Furthermore, some research has been done on the development of high-resolution NW-arrays for X-ray imaging [49,50]. There are also few reports on using single-nanowire devices for X-ray detection and beam shape characterization [51e53]. Consequently, using ZnO and PbI₂ materials in 1D hybrid nanostructures could potentially lead to next-generation high-resolution direct-conversion digital X-ray detector devices with advanced properties.

In this work, we demonstrate two different approaches to synthesize novel 1D ZnO/PbI₂ nanostructures. Highly crystalline few-layer PbI₂ was grown on ZnO NWs by: (1) direct thermal evaporation of PbI₂ powder, and (2) the conversion of a sputter-deposited lead oxide coating in iodine vapour at an elevated temperature. Two-terminal single-nanowire photodetectors were fabricated to show their enhanced photoelectric properties compared to pure ZnO NWs. The results show the potential of combining layered vdW materials with semiconducting nanowires to create novel nanostructures with advanced properties for potential photodetection applications. From our ab initio modelling, nanosized ZnO/PbI₂ heterostructures might be used for efficient photocatalytic hydrogen production from water.

2. Experimental details

2.1. Nanostructure synthesis and characterization

ZnO NWs were synthesised on oxidized silicon wafers SiO₂/Si(100) (Semiconductor Wafer, Inc.) via atmospheric pressure chemical vapour transport in an open-end horizontal quartz tube reactor using spherical Au nanoparticles (Smart materials, water suspension, 100 nm diameter) as a catalyst for the vapour-liquid-solid mechanism [54]. In short, 0.5 g of a 1:1 mixture of ZnO and carbon powders was loaded in a ceramic boat in the centre of the quartz tube at 900 C. The vapour was transported downstream to the Au/Si substrate at a lower temperature region using N₂ as a carrier gas. The temperature was held constant for 90 min, followed by natural cooling to the room temperature. See Fig. S1 for the scanning electron microscope (SEM) images and X-ray diffraction (XRD) pattern of the as-grown ZnO NWs.

In the next step, a few layers of PbI₂ were deposited on the as-grown ZnO NW arrays via two different approaches: (1) thermal evaporation of a PbI₂ powder and (2) sputter deposition of a lead

oxide coating followed by iodination at elevated temperatures. Both evaporation and sputtering were carried out in a Sidrabe SAF25/50 multifunctional cluster tool. In the first method, a simple thermal evaporation process was carried out in a vacuum chamber at 10⁻⁵ torr while rotating the ZnO NW sample (60 mg PbI₂ powder was evaporated from an Al₂O₃ crucible). The second method consists of two steps. First, a lead oxide PbO_x coating (consisting of different phases, including PbO and PbO₂ as shown by the XRD data in Fig. S2) was obtained by reactive DC magnetron sputtering of a metallic lead target in a mixed Ar/O₂ atmosphere (20 sccm Ar and 10 sccm O₂ gas flows, 5 min of sputtering at 100 W DC power). Second, as-prepared ZnO-PbO_x samples were annealed in a quartz tube in an iodine atmosphere for 15 min using an Ar/H₂ 5% mixture as the carrier gas to convert lead oxide to lead iodide. An iodine-rich atmosphere was obtained by placing 0.25 g iodine powder upstream of the sample at 120 C. The optimal annealing temperature was found to be 420 C, and the lead oxide conversion to PbI₂ starts around 350 C. One must optimize between a high coating crystallinity and the sublimation rate of the converted PbI₂ film, which increases rapidly above 400 C. As a reference sample for comparison, a PbI₂ thin film on SiO₂/Si substrate was prepared using the second approach.

The as-prepared nanostructure morphology was characterized using SEM-FIB (Lyra, Tescan), while the crystalline structure of the PbI₂ coating and ZnO NW was using a transmission electron microscope (TEM, Tecnai GF20, FEI) operated at a 200 kV accelerating voltage. The phase composition of the samples was studied using XRD (Q-Q Bragg Brentano powder diffractometer PANalytical X'Pert Pro) with monochromatic Cu K α irradiation and the spectra were analysed using PDXL2 software. Room-temperature photoluminescence (PL, Hamamatsu R92P PMT) spectra with a 266 nm excitation wavelength (fourth harmonic of CryLas Nd:YAG laser, 0.3 mJ power, 1 ns pulse duration, 5 kHz repetition rate) were measured to investigate the as-prepared nanostructure optical properties.

2.2. Single nanowire two-terminal photodetector device fabrication

To fabricate two-terminal single-nanowire photodetectors, first, gold microelectrodes with a 2 mm gap width were prepared on an oxidized silicon wafer by a conventional photolithography technique (see Fig. S3). The microelectrode array pattern was obtained using direct-write laser lithography (MPG101, Heidelberg Instruments) on Megaposit SPR700 photoresist (Rohm and Haas Electronic Materials), 5/45 nm Cr/Au film was deposited via thermal evaporation method followed by a lift-off procedure. Second, NWs were transferred onto the electrode array by mechanically pressing it to the substrate with the as-grown nanostructures, followed by welding selected single NWs to the corresponding underlying gold microelectrodes using electron-beam-assisted platinum deposition inside SEM-FIB to ensure the electric contact and fixed position. At least ten single-nanowire photodetectors (more than five for each synthesis method) were fabricated so consistent conclusions could be made.

2.3. Device measurements

Current voltage (IeV) characteristics and photoresponse of the fabricated single-NW photodetector devices were measured with a two-contact microprobe station connected to a low-noise current preamplifier (SR570, Stanford Research Systems) and oscilloscope (TDS2004B, Tektronix). A 405 nm wavelength semiconductor diode laser (CNI Laser) with 1 W/cm² power was the illumination source for the photoresponse measurements. An optical beam shutter (Thorlabs SH05) was used for time-resolved measurements. All the

measurements were performed at room temperature and in air.

2.4. Computational details

Total energy first-principle calculations for [0001]-oriented mono- (ML), bi- (2 ML) and three-layered (3 ML) PbI_2 nanosheets, and 24-layer thick [100] oriented slabs, to mimic the surface of ZnO nanowires, were performed using the HSE06 hybrid exchange-correlational functional [55] within the density functional theory (DFT), as implemented in the computer code CRYSTAL17 [56]. Localized Gaussian type functions (GTFs) in the form of atom-centred basis sets (BSs) for expansion of periodic crystalline orbitals for Zn and O were taken in the form of full electron Triple-Zeta Valence BS with polarization functions [56], while effective-core pseudopotential BS were taken for Pb and I [56]. The reliability of the chosen theoretical method were proven by calculations of bandgap energy (d) for bulk phase ZnO and PbI_2 crystals (see Fig. S5). The calculated bandgaps for all materials under study are in good agreement with those experimentally observed. To provide a balanced summation in both direct and reciprocal lattices, reciprocal space integration was performed by sampling the Brillouin zone (BZ) with a 6 6 1 Pack-Monkhorst mesh [57], which results in a total of 20 k-points evenly distributed over the BZs. For every fixed crystalline geometry calculation, the convergence was reached only when the total energy differed by less than

10^{-7} a.u. in two successive cycles of the self-consistent field (SCF) procedure [56]. Full geometry optimization was performed for all nanostructures considered in this study.

3. Results and discussion

3.1. Morphology, structure and photoluminescence measurements

SEM was used to image as-grown individual NWs and NW arrays and study their morphology. Pure ZnO NWs are typically 200-300 nm long with a diameter around 100 nm and exhibit a smooth surface (see Figs. S1(a and b)). Fig. 1(a and b) shows ZnO NWs with a thermally deposited PbI_2 coating. No significant change in diameter is observed; however, a very fine increase in surface roughness is visible. NWs with a sputter-deposited lead oxide coating with a fine roughness are shown in Fig. 1(c and d), where a

considerable (up to 100 nm) increase in diameter can be seen. After annealing such NWs in iodine vapour at elevated temperatures, the surface roughness greatly increased; however the diameter is significantly reduced as a fraction of the coated material is sublimated after the transformation (see Fig. 1(e and f)). The final coating is not uniform over the entire length of NWs as some thicker particles and islands can be observed. SEM images of the reference sample, PbI_2 thin film converted from sputter-deposited lead oxide, are shown in Fig. 1(g and h). The film exhibits hexagonal domains, presumably highly crystalline as PbI_2 typically crystallizes in a hexagonal structure.

A deeper insight into the nanostructures' inner structure was obtained using TEM. Fig. 2(a-e) shows TEM images of ZnO/PbI_2 NWs obtained by the thermal evaporation method at different magnifications. The lower resolution images show noticeable contrast between the two NW sides (PbI_2 layers correspond to the darker region), indicating non-uniform coating deposition, which is expected from the thermal evaporation approach since it is a line-of-sight method. At a high resolution, the crystalline structure of the nanostructure is revealed. The layers of PbI_2 grown on the ZnO NW surface are distinguishable as parallel black lines. Typically, the thickness of the coating varies between 5 and 10 monolayers (each consisting of 1 PbI_2 atomic planes), with interlayer distance measured around 7 Å, which is in a good agreement with the lattice constant ($a/4 = 6.979$ Å) of bulk hexagonal PbI_2 (ICDD-PDF #070235). Furthermore, the single-crystalline nature of the ZnO NWs is clearly visible; the measured interplanar distance is 2.8 Å, corresponding to hexagonal ZnO wurtzite (ICDD-PDF #361451), as confirmed by the XRD pattern (see Fig. S1(c)). The TEM images of the ZnO/PbI_2 nanostructures obtained by conversion of sputter-deposited lead oxide coating are shown in Fig. 2(d-f). In this case, the PbI_2 coating is uniformly distributed over the entire ZnO NW surface; however, the surface roughness is significantly increased. The thickness of the coating typically varies between 5 and 15 monolayers, with some islands being even thicker. As in to the first approach, the measured interlayer distance is around 7 Å.

To complement TEM structural investigations and confirm the presence of phases, XRD measurements were performed on the as-prepared samples. Fig. 3(a and b) show XRD patterns of NW arrays prepared by the two approaches: thermal evaporation and converting the magnetron-sputtered lead oxide coating, respectively.

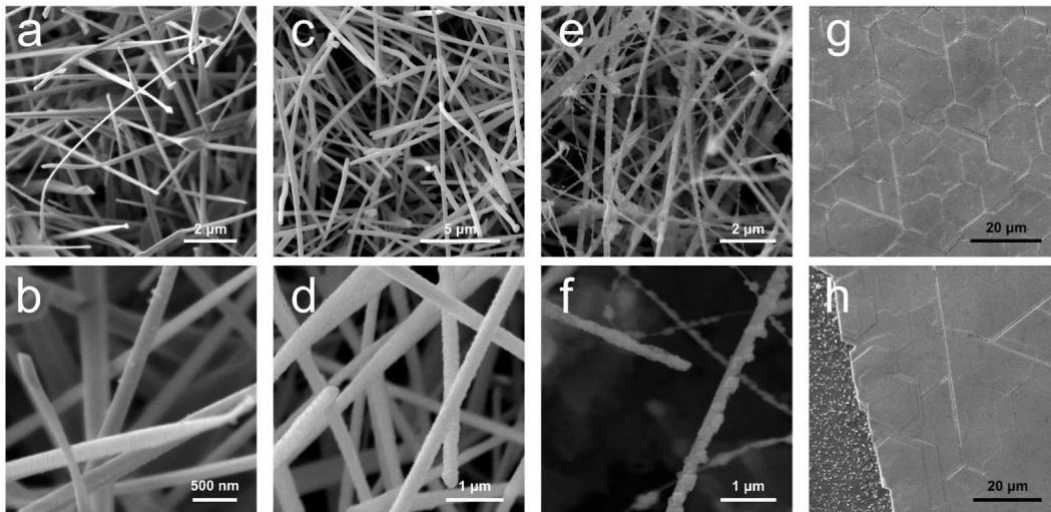


Fig. 1. Scanning electron microscope images of (a,b) ZnO/PbI_2 NWs made using the thermal evaporation approach; (c,d) ZnO NWs covered by lead oxide deposited by magnetron sputtering; (e,f) ZnO/PbI_2 NWs made by converting the lead oxide coating; (g,h) PbI_2 thin film made by converting a lead oxide film.

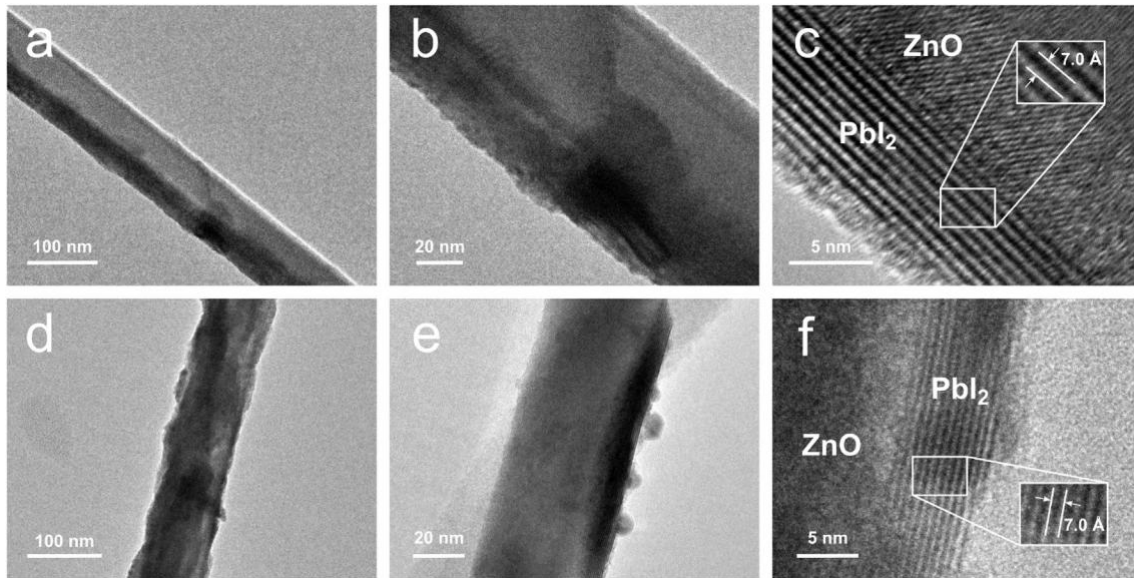


Fig. 2. Transmission electron microscope images at different magnifications of (a,b,c) ZnO-PbI₂ NWs made using the thermal evaporation approach, and (d,e,f) ZnO-PbI₂ NWs made by converting the magnetron-sputtered lead oxide coating. The insets show measured atomic interlayer distances between PbI₂ layers.

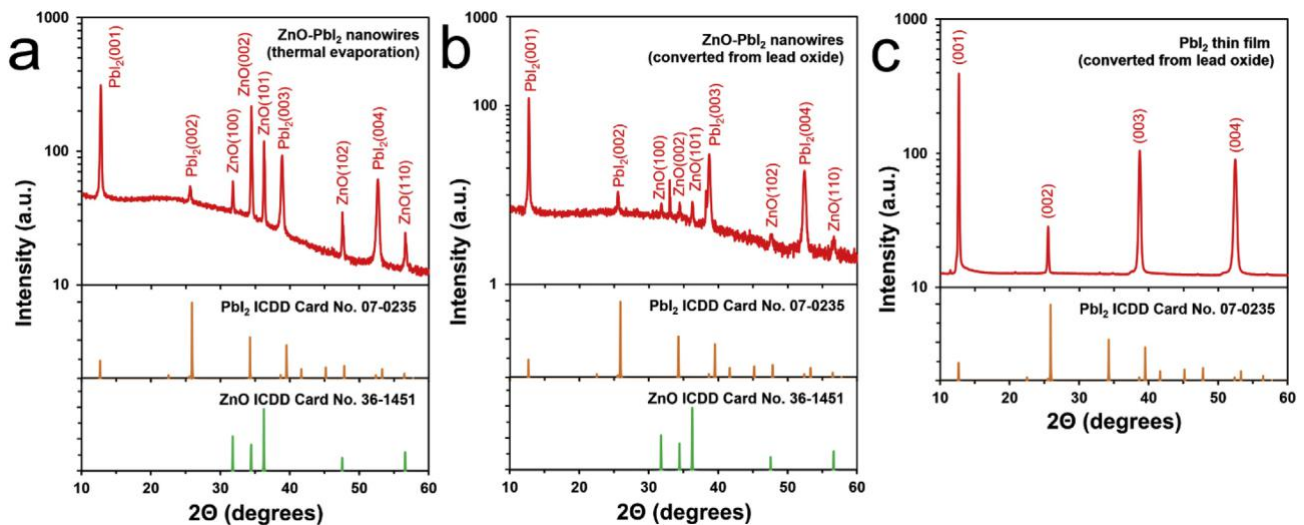


Fig. 3. X-ray diffraction patterns of (a) ZnO-PbI₂ NW arrays on Si/SiO₂ substrate made using the thermal evaporation approach; (b) ZnO-PbI₂ NW arrays on Si/SiO₂ substrate made by converting the magnetron-sputtered lead oxide coating; (c) PbI₂ thin film made by converting a lead oxide film.

Both patterns indicate highly crystalline hexagonal ZnO wurtzite (ICDD-PDF #361451) and hexagonal PbI₂ (ICDD-PDF #07e0235) phases. No other phases were observed, confirming the high crystallinity of the as-prepared nanostructures, as did the TEM investigations. It is worth noting that the ratio between PbI₂ and ZnO peak intensity is not only related to the amount of PbI₂ on ZnO NWs but also the amount of PbI₂ crystallites on the Si/SiO₂ substrate. Therefore, spectra cannot be properly used to describe the phase composition ratio in the nanostructures. Furthermore, ZnO NW Bragg peak intensities vary between the samples - due to an inhomogeneous gold nanoparticle catalyst deposition from colloid on the silicon substrate; the density of as-grown ZnO nanowires arrays was also not homogeneous while the PbI₂ layer is relatively homogeneous over the substrate due to the precisely controllable deposition method. In Fig. 3(b), the Bragg peak at 33 is attributed to diffraction in the Si(100) substrate (forbidden Si(200) reflection).

The XRD pattern of pure ZnO NWs is given in Fig. S1(c). The XRD pattern of the PbI₂ thin film reference sample shows its highly crystalline structure (see Fig. 3(c)), confirming that the conversion of a lead oxide film in iodine vapour is a viable method how to obtain crystalline PbI₂ thin films.

To study the optical properties, room temperature PL in the as-prepared samples was measured in a wavelength range from 400 to 650 nm, excited by a 266 nm laser. Generally, PbI₂ has a direct band-to-band transition at around 495 nm (~2.5 eV) [58]; however, a broad band peaked at 510-525 nm has been previously observed and attributed to recombination through defects, such as iodine and lead vacancies [25]. The PL spectrum of pure ZnO NWs exhibits a defect-related band at ~520 nm [16]. Therefore, the interpretation of the ZnO-PbI₂ nanostructure spectra might be ambiguous due to this ZnO and PbI₂ PL band overlapping, since higher ZnO PL intensities might lead to indistinguishable PbI₂ PL peaks or vice versa.

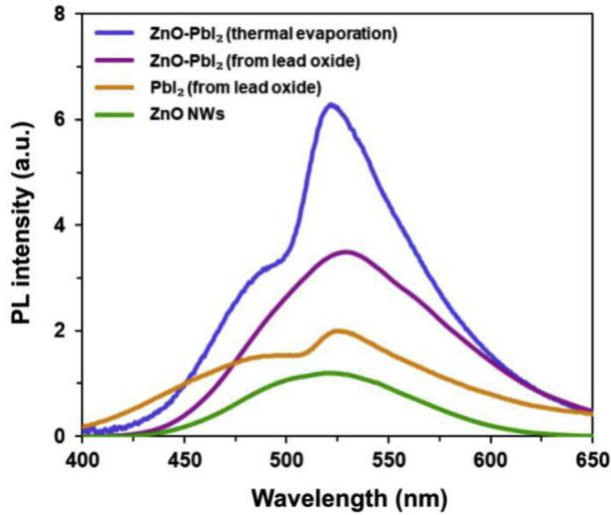


Fig. 4. Room temperature photoluminescence (PL) spectra at 266 nm excitation wavelength for the different as-prepared samples. The PL intensity is depicted in arbitrary units and does not contain information about relative intensities between the measured spectra.

Fig. 4 depicts our measured PL spectra of pure ZnO NWs, the PbI₂ thin film reference sample, and the ZnOePbI₂ nanostructures prepared via both approaches. It is worth noting that the PL intensity is depicted in arbitrary units and does not contain information about the relative intensities between the obtained spectra. The ZnO NW spectrum exhibits the typical defect band at 520 nm and the PbI₂ thin film sample (prepared by converting lead oxide film) shows two emission peaks: the direct band-to-band transition at around 495 nm and the defect-related band at around 530 nm. The ZnOePbI₂ nanostructures (prepared by thermal evaporation

approach) exhibit two peaks at 495 nm and 525 nm; however, the nanostructures prepared via lead oxide conversion exhibit only one band with a peak at 530 nm due to the higher intensity overlapping ZnO peak. One can see and interpret the difference between the PbI₂ peak ratio for samples prepared with different methods due to the defect-related peak maximum shift. For example, the defect/ band-to-band peak intensity ratio for thermally evaporated PbI₂ is ~2, while for lead oxide converted PbI₂, it is ~1.33. Therefore, by also considering the ZnO peak contribution, one can qualitatively assume that lead oxide conversion via iodination leads to fewer defects in PbI₂ coatings than the thermal evaporation approach.

3.2. Device photoresponse measurements

Two-terminal single-nanowire photodetectors were fabricated from the nanostructures prepared via both approaches, and pure ZnO NWs. Fig. 5(aec) shows the characteristics of the ZnOePbI₂ single NW devices made using the thermal evaporation approach, while Fig. 5(def) shows the characteristics of the ZnOePbI₂ single NW devices made by converting the magnetron-sputtered lead oxide coating (more than five single-nanowire photodetectors for each synthesis method were fabricated so that consistent conclusions could be made). The inset contains an SEM image of a typical as-prepared NW device. Both dark state current-voltage (IeV) characteristics of ZnOePbI₂ NWs in Fig. 5(a) and (d) exhibit linear behaviour, indicating that ohmic contacts formed between the nanostructures and the electrodes, as is expected for PbI₂ on gold [40,59] and which is beneficial for efficient photogenerated carrier collection. In contrast, pure ZnO NWs typically form Schottky contact with gold electrodes (see the nonsymmetric IeV curve in Fig. S4(a)) [60]. The devices were illuminated with 405 nm wavelength light in a periodic fashion to study their photoresponse properties as shown in Fig. 5(b) and

(e). All the devices were also tested for 532 nm and 660 nm light

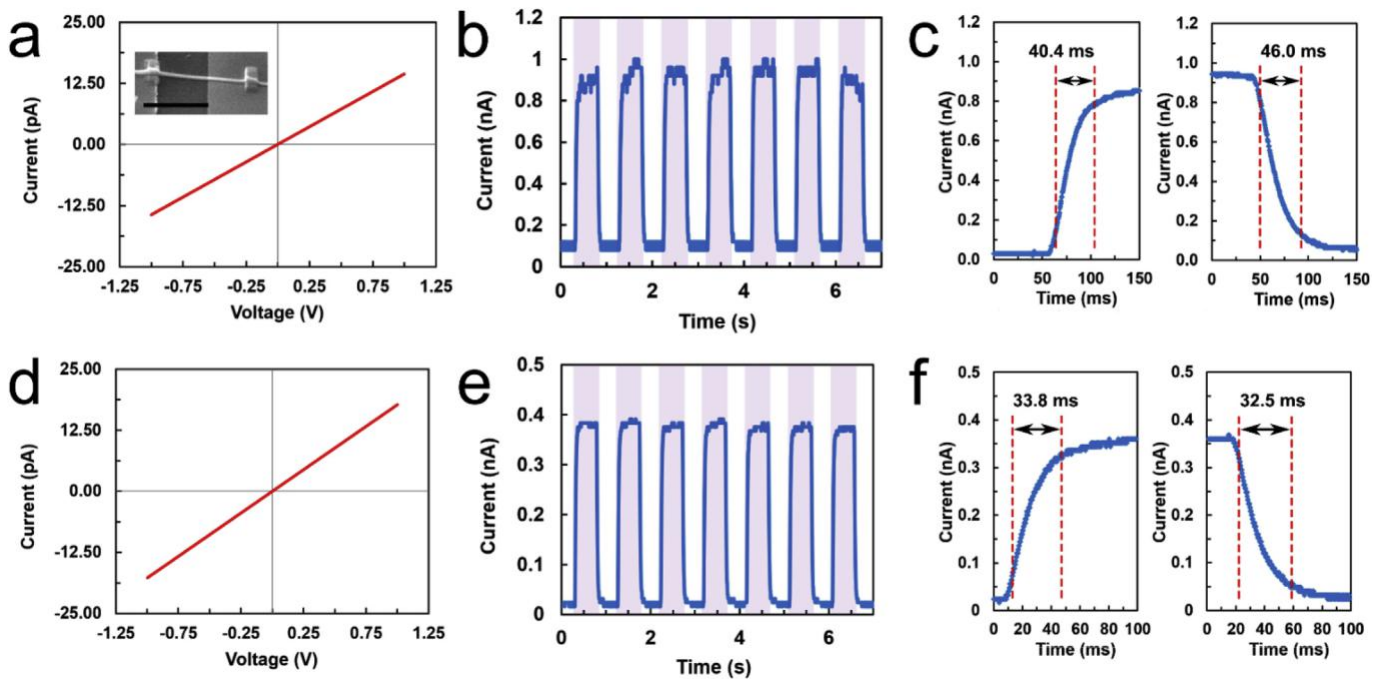


Fig. 5. ZnOePbI₂ single NW made using the thermal evaporation approach (a) dark state IeV characteristics, (b) on/off photoresponse, (c) time-resolved photoresponse measurements; and ZnOePbI₂ single NW made by converting the lead oxide coating (d) dark state IeV characteristics, (e) on/off photoresponse, (f) time-resolved photoresponse measurements at 1 V bias voltage and 1 W/cm² light intensity with 405 nm wavelength light. The inset shows an SEM image of a typical single-nanowire two-terminal photo-detector. The scale bar corresponds to 2 nm.

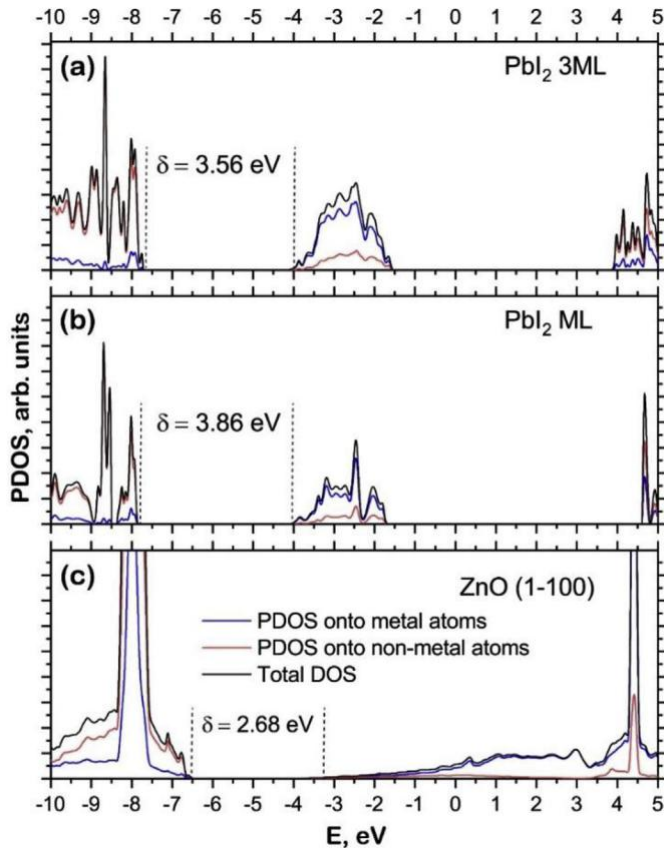


Fig. 6. Total and projected densities of states (PDOS) calculated for (a) 3-monolayer thick PbI₂ nanosheet, (b) monolayer thick PbI₂ nanosheet, and (c) ZnO (1e100) slab. The 24-layer thick slab of ZnO substrate is symmetrically terminated to mimic the surface of the nanowires. PDOS projected onto all orbitals of corresponding metal or non-metal atoms. The energy scale is shown with respect to the vacuum level.

illumination; however, no increase in current was observed due to the relatively wide bandgap of the studied materials. On-off measurements demonstrate a steady, rapid and repeatable increase and decrease of the current when the illumination is turned on or off, respectively; therefore, showing good stability and reversibility of the devices. ZnOePbI₂ NWs exhibit low dark current (10e100 pA) which is necessary for high-performance photodetectors, while for pure ZnO NWs, it can be up to several tens of nA (see Fig. S4(b)). The current enhancement ratios (I_{on}/I_{off}) for the nanostructures prepared via both approaches were measured to be at around 10e20, in contrast to less than 2 for pure ZnO NWs. Time-resolved photoresponse measurements were performed to evaluate the rise and decay time of the as-prepared ZnOePbI₂ devices, defined as the required time for the photocurrent to increase or decrease to 90% or 10% of its maximum value, respectively. As shown in Fig. 5(c) and (f), the obtained values are in the 30e50 ms range, which is almost two orders of magnitude faster than the pure ZnO NWs (see Fig. S4(c)) and comparable to typical NW or 2D PbI₂ photodetector response times [35,41,42,59,61]. The slow response of ZnO NWs is due to the influence of oxygen molecules on the surface states and their effect on photoresponse kinetics is widely discussed in the literature [62,63]. Here and in our previous work [20], we passivated the surface of ZnO NWs using a thin PbI₂ or WS₂ coating, respectively, and photodetectors of such heterostructures exhibit reduced dark current and photoresponse time, although it also decreased on-state current I_{on} in comparison to pure ZnO NWs. It

is well known that adsorbed oxygen species influence electrical properties (electrical conductivity decreases with exposure to oxygen) of metal oxide nanostructures [11,64e66]. Consequently, band bending, induced by adsorbed oxygen molecules that capture free electrons, causes an efficient photogenerated electron-hole separation that leads to high gain in single-nanowire photodetectors. The presence of the PbI₂ layers in our nanostructures protects the ZnO surface from oxygen adsorption that might influence surface-related photoinduced processes and decrease the number of charge carrier trapping centres.

The thickness of PbI₂ on ZnO NWs, which were used in the as-fabricated photodetector devices, was typically 6e13 layers. No significant changes in the photodetector characteristics, such as spectral responsivity R_l , response time or current enhancement ratios (I_{on}/I_{off}), were observed between the samples in this PbI₂ thickness range. It is worth noting, that there are theoretical and experimental studies that show a band structure shift from direct bandgap to indirect bandgap when the PbI₂ thickness is reduced from bulk to monolayer [35,38]; therefore, monolayer PbI₂ is not expected to be an efficient material for optoelectronics applications and few-layer PbI₂ should be used instead.

Spectral responsivity (R_l) and external quantum efficiency (EQE) are used to evaluate photoconductive properties of a material. R_l and EQE are respectively defined as $R_l = \frac{1}{4} \frac{DI}{(PS)}$ and $EQE = \frac{1}{4} \frac{hcR_l}{(el)}$ [40], where DI is the difference between the photocurrent I_{on} and the dark current I_{off} , P is the light power density, S is the effective illumination area (estimated as the electrode gap width NW diameter), h is Planck's constant, c is the speed of light, e is the electron charge and l is the light wavelength. Large R_l and EQE values correspond to high photodetector sensitivity. A responsivity as high as ~0.6 A/W (EQE ~180%) was calculated for the ZnOePbI₂ single NW devices made using the thermal evaporation approach and ~0.3 A/W (EQE ~90%) for the ones made by converting the magnetron-sputtered lead oxide coating; however, it is not valid to compare the two different synthesis approaches based only on the responsivity values as the value range for all as-fabricated devices overlapped no matter which method was used. The obtained R_l and EQE values are comparable to other typical state-of-the-art 1D nanostructure [61] and 2D PbI₂ [41,42,44,59] photodetectors.

3.3. Electronic structure calculations

Fig. 6 compares the total and projected densities of states (PDOS) calculated for [0001]-oriented monolayered (ML) and three-layered (3 ML) PbI₂ nanosheets, Fig. 6(a) and (b), respectively, and the PDOS calculated for slab models of [1e100] oriented ZnO NW (Fig. 6(c)). The PDOS calculated for bi-layered (2 ML) PbI₂ nanosheet is not presented in Fig. 6 since its electronic structure does not practically differ from that calculated for 3 ML PbI₂. For all PbI₂ nanosheets under study, the upper part of the valence band (VB) is predominantly formed by the iodine (5p) orbitals with significant contributions from lead (6s) orbitals. The bottom of the conduction band (CB) of PbI₂ nanosheets is formed mainly from Pb (6p) states. In the case of ZnO (1e100) surfaces, the VB top is formed by oxygen 2p states, while 3d orbitals of Zn mainly form the CB bottom. The band edge positions of ML and 3 ML PbI₂ differ from those of bulk (Fig. S5(a)). The bottom of the CB is shifted down, closer to the hydrogen evolution potential of 4.44 eV. The position of the top of the VB calculated for (1e100) ZnO NW surfaces is located near 5.67 eV oxygen reduction potential, which allows us to conclude that the hybrid ZnOePbI₂ NWs can be considered as promising potential materials for efficient solar-driven photo (electro)catalytic water splitting.

4. Conclusions

In this paper, we demonstrated for the first time the growth of ZnO NWs decorated with highly crystalline few-layer PbI₂ and fabricated two-terminal single-nanowire photodetector devices to investigate the photoelectric properties of the hybrid ZnO@PbI₂ nanostructures. We developed a novel two-step growth process for uniform crystalline PbI₂ nanosheets via reactive magnetron deposition of a lead oxide film followed by subsequent iodination in iodine vapour to PbI₂ at 420 °C on a ZnO NW substrate, and we compared as-grown hybrid nanostructures with ones prepared via thermal evaporation method. As-prepared two-terminal single-nanowire ZnO@PbI₂ photodetectors are comparable to state-of-the-art 1D nanostructure and 2D PbI₂ photodetectors and exhibit enhanced optoelectronic characteristics, such as reduced dark current and significantly decreased photoresponse time compared to pure ZnO NWs, and have responsivity up to 0.6 A/W. We found that the preparation method does not significantly affect the photoelectric properties of the nanostructures; however, PbI₂ obtained by thermal evaporation benefits from a smoother coating and, presumably, less optical defect states, but lacks the uniform coverage of PbI₂ converted from lead oxide coating. First principle DFT calculations on few-layer PbI₂ nanosheets, thin slabs to mimic the surface of ZnO NWs, and bulk phase ZnO and PbI₂ crystals, were performed to obtain the electronic structure of the materials under study. The results show the potential of combining layered vdW materials with semiconducting nanowires to create novel nano-structures with enhanced properties for applications in optoelectronics or X-ray detectors. Our ab initio modelling also shows that nanosized ZnO@PbI₂ heterostructures might be used for efficient photocatalytic and electrocatalytic hydrogen production from water.

Declaration of competing interest

There are no conflicts of interest to declare.

CRediT authorship contribution statement

Edgars Butanovs: Methodology, Validation, Investigation, Visualization, Writing - original draft. Sergei Piskunov: Methodology, Formal analysis, Visualization. Aleksejs Zolotarjovs: Investigation. Boris Polyakov: Conceptualization, Supervision, Investigation, Writing - review & editing.

Acknowledgements

Financial support provided by Scientific Research Project for Students and Young Researchers Nr. SJZ/2017/1 realized at the Institute of Solid State Physics, University of Latvia is greatly acknowledged. The authors are grateful to Liga Bikse for XRD measurements.

References

- [1] J. Wen, et al., Photocatalysis fundamentals and surface modification of TiO₂ nanomaterials, *Chin. J. Catal.* 36 (2015) 2049e2070.
- [2] Y. Guo, K. Xu, C. Wu, J. Zhao, Y. Xie, Surface chemical-modification for engineering the intrinsic physical properties of inorganic two-dimensional nanomaterials, *Chem. Soc. Rev.* 44 (2015) 637e646.
- [3] A. Pescaglini, D. Iacopino, Metal nanoparticle@semiconductor nanowire hybrid nanostructures for plasmon-enhanced optoelectronics and sensing, *J. Mater. Chem. C* 3 (2015) 11785e11800.
- [4] R. Yan, D. Gargas, P. Yang, Nanowire photonics, *Nat. Photon.* 3 (2009) 569e576.
- [5] Y. Li, F. Qian, J. Xiang, C.M. Lieber, Nanowire electronic and optoelectronic devices, *Mater. Today* 9 (2006) 18e27.
- [6] L.J. Lauhon, M.S. Gudiksen, D. Wang, C.M. Lieber, Epitaxial core@shell and core@multishell nanowire heterostructures, *Nature* 420 (2002) 57e61.
- [7] Y. Dong, B. Tian, T.J. Kempa, C.M. Lieber, Coaxial group III Nitride nanowire photovoltaics, *Nano Lett.* 9 (2009) 2183e2187.
- [8] T.J. Kempa, R.W. Day, S.-K. Kim, H.-G. Park, C.M. Lieber, Semiconductor nanowires: a platform for exploring limits and concepts for nano-enabled solar cells, *Energy Environ. Sci.* 6 (2013) 719.
- [9] W. Tian, D. Liu, F. Cao, L. Li, Hybrid nanostructures for photodetectors, *Adv. Opt. Mater.* 5 (2017) 1600468.
- [10] Y. Zhang, M.K. Ram, E.K. Stefanakos, D.Y. Goswami, Synthesis, characterization, and applications of ZnO nanowires, *J. Nanomater.* 1e22 (2012), 2012.
- [11] C. Soci, et al., ZnO nanowire UV photodetectors with high internal gain, *Nano Lett.* 7 (2007) 1003e1009.
- [12] Z.L. Wang, Piezoelectric nanogenerators based on zinc oxide nanowire arrays, *Science* 312 (2006) 242e246.
- [13] M.J.F. Empizo, et al., Photoluminescence properties of a single ZnO micro-structure for potential scintillator applications, *Opt. Mater. (Amst.)* 38 (2014) 256e260.
- [14] P.J. Simpson, R. Tjossem, A.W. Hunt, K.G. Lynn, V. Munne, Superfast timing performance from ZnO scintillators, *Nucl. Instrum. Methods Phys. Res. Sect. A Accel. Spectrom. Detect. Assoc. Equip.* 505 (2003) 82e84.
- [15] P.A. Rodnyi, I.V. Khodyuk, Optical and luminescence properties of zinc oxide (Review), *Optic Spectrosc.* 111 (2011) 77e785.
- [16] Ü. Özgür, et al., A comprehensive review of ZnO materials and devices, *J. Appl. Phys.* 98 (2005), 041301.
- [17] Z.L. Wang, ZnO nanowire and nanobelt platform for nanotechnology, *Mater. Sci. Eng. R Rep.* 64 (2009) 33e71.
- [18] H. Liu, Z. Feng, J. Wang, J. Diao, D. Su, Synthesis of hollow carbon nano-structures using a ZnO template method, *N. Carbon Mater.* 31 (2016) 87e91.
- [19] K. Liu, M. Sakurai, M. Liao, M. Aono, Giant improvement of the performance of ZnO nanowire photodetectors by Au nanoparticles, *J. Phys. Chem. C* 114 (2010) 19835e19839.
- [20] E. Butanovs, et al., Fast-response single-nanowire photodetector based on ZnO/WS₂ core/shell heterostructures, *ACS Appl. Mater. Interfaces* 10 (2018) 13869e13876.
- [21] A. Pescaglini, et al., Hot-electron injection in Au nanorod@ZnO nanowire hybrid device for near-infrared photodetection, *Nano Lett.* 14 (2014) 6202e6209.
- [22] O. Lupan, V. Postica, T. Pauporte, M. Hoppe, R. Adelung, UV nano-photodetectors: a case study of individual Au-modified ZnO nanowires, *Sensor Actuator Phys.* 296 (2019) 400e408.
- [23] J. Grottrup, et al., UV detection properties of hybrid ZnO tetrapod 3-D networks, *Vacuum* 146 (2017) 492e500.
- [24] H.-M. Kim, J.-H. Park, S.-K. Lee, Fiber optic sensor based on ZnO nanowires decorated by Au nanoparticles for improved plasmonic biosensor, *Sci. Rep.* 9 (2019) 15605.
- [25] J. Zhang, et al., Layered ultrathin PbI₂ single crystals for high sensitivity flexible photodetectors, *J. Mater. Chem. C* 3 (2015) 4402e4406.
- [26] Y. Fu, et al., Metal halide perovskite nanostructures for optoelectronic applications and the study of physical properties, *Nat. Rev. Mater.* 4 (2019) 169e188.
- [27] H.L. Zhu, et al., Achieving high-quality SnPb perovskite films on complementary metal-oxide-semiconductor-compatible metal/silicon substrates for efficient imaging array, *ACS Nano* 13 (2019) 11800e11808.
- [28] H.L. Zhu, et al., Low-bandgap methylammonium-rubidium cation Sn-rich perovskites for efficient ultraviolet-visible-near infrared photodetectors, *Adv. Funct. Mater.* 28 (2018) 1706068.
- [29] H.L. Zhu, et al., Room-temperature solution-processed NiOx:PbI₂ nano-composite structures for realizing high-performance perovskite photodetectors, *ACS Nano* 10 (2016) 6808e6815.
- [30] F. Ye, et al., High-quality cuboid CH₃NH₃PbI₃ single crystals for high performance X-ray and photon detectors, *Adv. Funct. Mater.* 29 (2019) 1806984.
- [31] K. Shah, et al., Lead iodide X-ray detection systems, *Nucl. Instrum. Methods Phys. Res. Sect. A Accel. Spectrom. Detect. Assoc. Equip.* 380 (1996) 266e270.
- [32] J.F. Condeles, et al., Fabrication and characterization of thin films of PbI₂ for medical imaging, *J. Non-Cryst. Solids* 338e340 (2004) 81e85.
- [33] X.H. Zhu, Z.R. Wei, Y.R. Jin, A.P. Xiang, Growth and characterization of a PbI₂ single crystal used for gamma ray detectors, *Cryst. Res. Technol.* 42 (2007) 456e459.
- [34] H. Sun, et al., Laser-induced surface recrystallization of polycrystalline PbI₂ thick films for X-ray detector application, *Appl. Surf. Sci.* 427 (2018) 1146e1151.
- [35] M. Zhong, et al., Large-scale 2D PbI₂ monolayers: experimental realization and their indirect band-gap related properties, *Nanoscale* 9 (2017) 3736e3741.
- [36] D.L. Duong, S.J. Yun, Y.H. Lee, van der Waals layered materials: opportunities and challenges, *ACS Nano* 11 (2017) 11803e11830.
- [37] W. Choi, et al., Recent development of two-dimensional transition metal dichalcogenides and their applications, *Mater. Today* 20 (2017) 116e130.

- [38] A.S. Toulouse, et al., Frenkel-like Wannier-Mott excitons in few-layer PbI₂, *Phys. Rev. B* 91 (2015) 165308.
- [39] A. Splendiani, et al., Emerging photoluminescence in monolayer MoS₂, *Nano Lett.* 10 (2010) 1271e1275.
- [40] M. Zhong, et al., Flexible photodetectors based on phase dependent PbI₂ single crystals, *J. Mater. Chem. C* 4 (2016) 6492e6499.
- [41] W. Zheng, et al., High-crystalline 2D layered PbI₂ with ultrasoft surface: liquid-phase synthesis and application of high-speed photon detection, *Adv. Electron. Mater.* 2 (2016) 1600291.
- [42] Y. Wang, L. Gan, J. Chen, R. Yang, T. Zhai, Achieving highly uniform two-dimensional PbI₂ flakes for photodetectors via space confined physical va-por deposition, *Sci. Bull.* 62 (2017) 1654e1662.
- [43] J. Liu, et al., Synthesis of PbI₂ nanowires for high sensitivity photodetectors, *RSC Adv.* 6 (2016) 59445e59449.
- [44] J. Zhang, et al., Low-temperature heteroepitaxy of 2D PbI₂/graphene for large-area flexible photodetectors, *Adv. Mater.* 30 (2018) 1803194.
- [45] B. Polyakov, et al., Unexpected epitaxial growth of a few WS₂ layers on {1100} facets of ZnO nanowires, *J. Phys. Chem. C* 120 (2016) 21451e21459.
- [46] E. Butanovs, A. Kuzmin, J. Butikova, S. Vlassov, B. Polyakov, Synthesis and characterization of ZnO/ZnS/MoS₂ core-shell nanowires, *J. Cryst. Growth* 459 (2017) 100e104.
- [47] F. Chen, T. Wang, L. Wang, X. Ji, Q. Zhang, Improved light emission of MoS₂ monolayers by constructing AlN/MoS₂ core-shell nanowires, *J. Mater. Chem. C* 5 (2017) 10225e10230.
- [48] Z. Fan, et al., Toward the development of printable nanowire electronics and sensors, *Adv. Mater.* 21 (2009) 3730e3743.
- [49] M. Kobayashi, et al., Development of vertically aligned ZnO-nanowires scin-tillators for high spatial resolution x-ray imaging, *Appl. Phys. Lett.* 106 (2015), 081909.
- [50] A. Taheri, S. Saramad, S. Setayeshi, ZnO nanowires in polycarbonate mem-brane as a high resolution X-ray detector (a Geant4 simulation), *Nucl. Instrum. Methods Phys. Res. Sect. A Accel. Spectrom. Detect. Assoc. Equip.* 716 (2013) 15e22.
- [51] J. Wallentin, et al., Hard X-ray detection using a single 100 nm diameter nanowire, *Nano Lett.* 14 (2014) 7071e7076.
- [52] J. Wallentin, M. Osterhoff, T. Salditt, In operando X-ray nanodiffraction reveals electrically induced bending and lattice contraction in a single nanowire de-vice, *Adv. Mater.* 28 (2016) 1788e1792.
- [53] A. Johannes, et al., In operando X-ray imaging of nanoscale devices: compo-sition, valence, and internal electrical fields, *Sci. Adv.* 3 (2017) eaao4044.
- [54] P. Yang, et al., Controlled growth of ZnO nanowires and their optical prop-erties, *Adv. Funct. Mater.* 12 (2002) 323.
- [55] J. Heyd, G.E. Scuseria, M. Ernzerhof, Hybrid functionals based on a screened Coulomb potential, *J. Chem. Phys.* 118 (2003) 8207e8215.
- [56] R. Dovesi, et al., Quantum-mechanical condensed matter simulations with CRYSTAL, *Wiley Interdiscipl. Rev. Comput. Mol. Sci.* 8 (2018), e1360.
- [57] H.J. Monkhorst, J.D. Pack, Special points for Brillouin-zone integrations, *Phys. Rev. B* 13 (1976) 5188e5192.
- [58] J.F. Condeles, R.A. Ando, M. Mulato, Optical and structural properties of PbI₂ thin films, *J. Mater. Sci.* 43 (2008) 525e529.
- [59] C. Lan, et al., Large-scale synthesis of freestanding layer-structured PbI₂ and MAPbI₃ nanosheets for high-performance photodetection, *Adv. Mater.* 29 (2017) 1702759.
- [60] C.S. Lao, et al., ZnO nanobelt/nanowire Schottky diodes formed by dielec-trophoresis alignment across Au electrodes, *Nano Lett.* 6 (2006) 263e266.
- [61] T. Zhai, et al., Recent developments in one-dimensional inorganic nano-structures for photodetectors, *Adv. Funct. Mater.* 20 (2010) 4233e4248.
- [62] G. Cheng, et al., ZnO nanowire Schottky barrier ultraviolet photodetector with high sensitivity and fast recovery speed, *Appl. Phys. Lett.* 99 (2011) 203105.
- [63] B. Mallampati, S.V. Nair, H.E. Ruda, U. Philipose, Role of surface in high photoconductive gain measured in ZnO nanowire-based photodetector, *J. Nanoparticle Res.* 17 (2015) 176.
- [64] J.-M. Wu, C.-H. Kuo, Ultraviolet photodetectors made from SnO₂ nanowires, *Thin Solid Films* 517 (2009) 3870e3873.
- [65] N. Yamazoe, J. Fuchigami, M. Kishikawa, T. Seiyama, Interactions of tin oxide surface with O₂, H₂O AND H₂, *Surf. Sci.* 86 (1979) 335e344.
- [66] S.C. Chang, Oxygen chemisorption on tin oxide: correlation between electrical conductivity and epr measurements, *J. Vac. Sci. Technol.* 17 (1979) 366e369.